Journal of Neuroimmunology 334 (2019) 576995

Contents lists available at ScienceDirect

Journal of Neuroimmunology

journal homepage: www.elsevier.com/locate/jneuroim

Short Communication

Experimental autoimmune encephalomyelitis accelerates remyelination after lysophosphatidylcholine-induced demyelination in the corpus callosum

Anna-Claire Lamport[a], Matthew Chedrawe[a], Matthew Nichols[a], George S. Robertson[a,b,*]

[a] Department of Pharmacology, Brain Repair Centre, Faculty of Medicine, Dalhousie University, 1348 Summer Street, Life Sciences Research Institute, North Tower, Halifax B3H 4R2, Canada

[b] Department of Psychiatry, Brain Repair Centre, Faculty of Medicine, Dalhousie University, 1348 Summer Street, Life Sciences Research Institute, North Tower, Halifax B3H 4R2, Canada

A B S T R A C T

Experimental autoimmune encephalomyelitis (EAE) and lysophosphatidylcholine (LPC)-induced demyelination were combined to study remyelination in a pro-inflammatory context. Two groups of female C57BL/6 mice were subjected either to EAE (EAE mice) or injected with just complete Freund's adjuvant (CFA) and pertussis toxin (PTX) followed by bilateral LPC and phosphate buffered saline injections in the corpus callosum on day 7 (CFA controls). Relative to CFA controls, EAE accelerated remyelination and increased innate immune cell activation, lymphocyte infiltration and cytokine gene expression in the LPC lesions. However, compared to CFA mice, remyelination was reduced (day 14) suggesting this aggressive immune response also compromised myelin repair in EAE mice.

1. Introduction

Remyelination is considered essential for functional recovery in multiple sclerosis (MS) (Duncan et al., 2009; Franklin and Gallo, 2014). However, myelin repair in MS is known to fail (Franklin, 2002). This places a massive metabolic burden on axons causing irreversible damage responsible for permanent neurological deficits in MS (Trapp et al., 1998; Trapp and Stys, 2009). Understanding how this occurs is critical to the development of restorative therapies that oppose MS disease progression (Fancy et al., 2010). MS lesions are characterized by immune cell infiltration, microglial activation, astrogliosis and axonal damage (Frischer et al., 2009; Henderson et al., 2009). However, the precise mechanisms by which these pro-inflammatory processes regulate myelin repair are not yet clear. Autoimmune-mediated or toxin-induced demyelination models have typically been employed to study remyelination in mice. EAE, induced by immunizing mice with myelin oligodendrocyte glycoprotein 35–55 ($MOG_{35–55}$), reproduces spinal cord immune cell infiltration, microglial activation, astrogliosis, demyelination and axonal injury seen in MS (Jones et al., 2008; Steinman and Zamvil, 2006). However, the sporadic nature of these pathological processes combined with their failure to involve forebrain white matter as seen in MS are major limitations of the EAE model.

A commonly used model of toxin-induced demyelination employs stereotaxic injection of concentrated lysophosphatidylcholine (LPC) into the central nervous system (CNS). Injection of LPC produces a focal demyelinating lesion that peaks in size about 24 to 72 h (hr) later. Remyelination begins 7 days post-injection, with near-complete remyelination occurring after 3 weeks (Hall, 1972). LPC primarily causes lysis of myelin membranes, sparing underlying axons (Keough et al., 2015). Axons are largely uninjured because the immune response following LPC-induced demyelination is modest (Hoflich et al., 2016; Schultz et al., 2017). This model therefore fails to mimic immune-mediated white matter loss and remyelination deficits typical of MS.

Although $MOG_{35–55}$-induced EAE does not promote demyelination in the corpus callosum, pro-inflammatory cytokine elevations and immune activation do occur in the forebrain (Chanaday and Roth, 2016). This suggests that demyelination in the corpus callosum of EAE mice may model immune events that regulate remyelination in MS. We therefore compared remyelination, immune infiltration and cytokine mRNA levels within the PBS and LPC injection sites of CFA control and EAE mice.

2. Methods

2.1. Dual EAE and LPC model

Thirty-two female C57L/6 mice (10–12 weeks) underwent EAE induction and 32 were immunized with complete Freund's adjuvant (CFA) according to our previously described methods (Chedrawe et al., 2018). Seven days following injection of MOG, all mice in both groups received injections of PBS and LPC into the corpus callosum of the left and right hemisphere (both 1.0 mm rostral, 1.0 mm lateral and 2.3 mm

* Corresponding author at: Department of Pharmacology, Brain Repair Centre, Faculty of Medicine, Dalhousie University, 1348 Summer Street, Life Sciences Research Institute, North Tower, Halifax B3H 4R2, Canada.

E-mail address: robertgs@dal.ca (G.S. Robertson).

https://doi.org/10.1016/j.jneuroim.2019.576995

Received 9 April 2019; Received in revised form 13 June 2019

0165-5728/ © 2019 Elsevier B.V. All rights reserved.

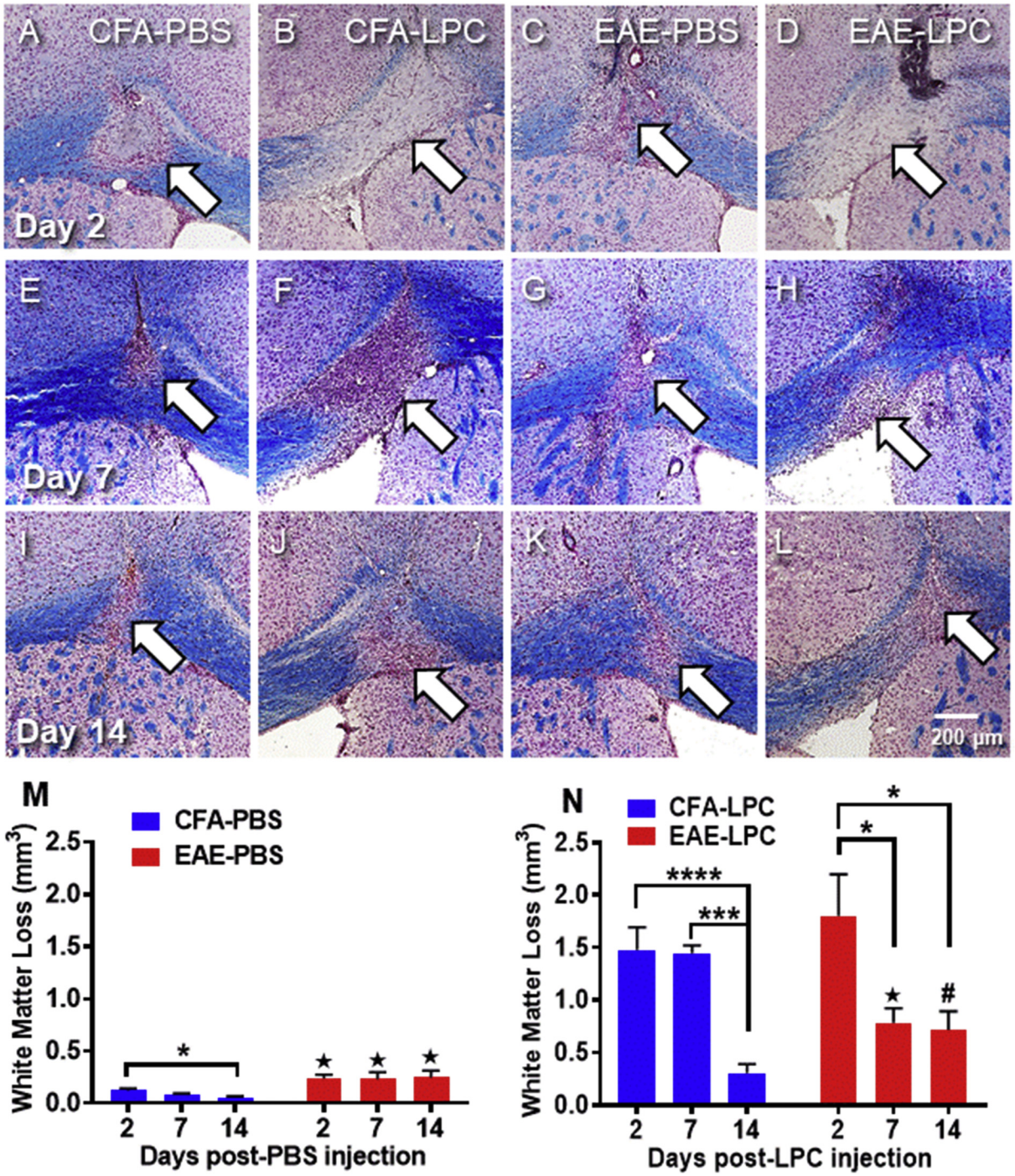

Fig. 1. Eriochrome cyanine/neutral red (EC/NR) staining of representative lesions from CFA and EAE mice 2 (A–D), 7 (*E*-H) and 14 (I–L) days following stereotaxic injection of LPC (n = 8 mice/group/time point, 3 CFA mice excluded at day 7 due to inadequate injection of LPC). (M) Mean volume of white matter loss within the corpus callosum at 2, 7 and 14 days following PBS injection in CFA or EAE mice. *$p < 0.05$; ⋆p < 0.05 compared to day 2, 7 and 14 CFA-LPC mice (N) Mean volume of white matter loss within the corpus callosum 2, 7 and 14 days following LPC injection in CFA or EAE mice. *p < 0.05, ***$p < 0.001$, ****$p < 0.0001$, ⋆p < 0.001 compared to day 7 CFA-LPC, #p < 0.05 compared to day 14 CFA LPC, one-way ANOVA followed by Tukey's post hoc test. (For interpretation of the references to colour in this figure legend, the reader is referred to the web version of this article.)

ventral to bregma) in the same manner described previously (Warford et al., 2018). The needle was left in place for 3 min following injection to reduce backflow. Three CFA/PTX mice were excluded from the analysis due to inadequate LPC injections. Beginning on the day of LPC injection, all mice were assigned a clinical score to assess motor deficits according to our previously described methods (Chedrawe et al., 2018).

2.2. Tissue collection, processing and sectioning for histology

Mice were humanely killed by an overdose intra-peritoneal injection (i.p.) of pentobarbital (150 mg/kg) 2, 7, or 14 days (n = 8/group/day) following injection of LPC. Following perfusion, brains were removed and allowed to post-fix in 4% paraformaldehyde for 48 h. Each brain was cryoprotected in 15% then 30% sucrose dissolved in PBS. Once the brain had sunk in 30% sucrose, 20 µm thick coronal sections were cut

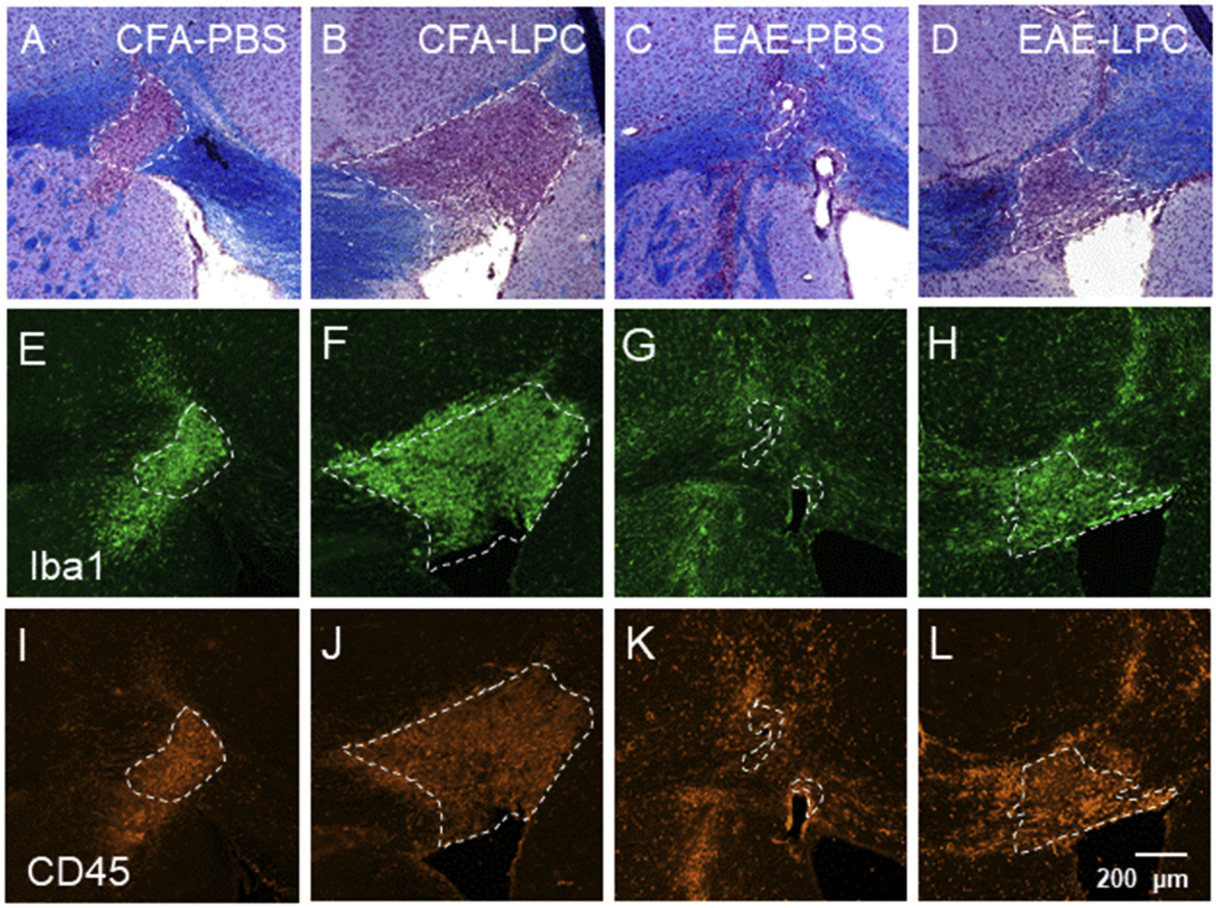

Fig. 2. (A–D) Eriochrome cyanine staining 7 days after the injection of PBS (A and C) and LPC (B and D) injections in the corpus callosum of CFA and EAE mice. Iba1 (E–H) and CD45 (I–L) immunoreactivities in adjacent sections (n = 8 mice/group, 3 CFA mice excluded due to inadequate injection of LPC).

using a cryostat, placed on SuperFrost slides and stored at −20 °C.

2.3. Erichrome cyanine and neutral red staining

Every second section from each brain was stained with eriochrome cyanine and counterstained with neutral red (EC/NR) as described previously (Chedrawe et al., 2018).

2.4. Immunohistochemistry

Sections were rehydrated with 0.5% Triton X-100 in PBS (T-PBS). Myelin was visualized by the incubation of sections with FluoroMyelin Green (1:100, ThermoFisher) for 20 min, followed by three 3-minute washes with T-PBS. Additional sections were blocked with 10% Goat serum and 10% Donkey serum in T-PBS for 1 h at room temperature and then incubated with the primary antibodies diluted in T-PBS for 18 h at 4 °C with the following primary antibodies: Rabbit anti-Iba1 (1:500, Wako Pure Chemical Industries) and rat anti-CD45 (1:12, BD Pharmingen). The next day, sections were washed and incubated with the following secondary antibodies diluted in T-PBS: Goat anti-Rabbit IgG AlexaFluor 488 (1:500; ThermoFisher) or donkey anti-Rat IgG AlexaFluor 594 (1:500, ThermoFisher). Sections were then washed and cover-slipped using Fluoromount mounting medium. Slides were sealed with nail polish and imaged at 100× magnification using the Zeiss AxioImager Z2.

2.5. Modified cavalieri method of white matter loss quantification

A total of 40 serial sections from 0.4 mm rostral to 1.2 mm caudal of the needle tract stained with EC/NR were assessed for white matter loss in the corpus callosum of each mouse (n = 8/group). Using Fiji (ImageJ) software, a grid of crosses, each associated with an area of 500 µm^2, was placed over the image and the number of crosses overlaying a region of white matter loss was counted. The number of crosses was multiplied by 1000 µm^2 (area associated with cross x sections thickness - 500 µm^2 × 20 µm^2). These values were used to plot lesion size (Y axis) against distance from the injection site (X axis) for each lesion. Using Prism 7 software, the area under each of these curves was summed to obtain the volume of white matter loss.

2.6. Quantitative RT-PCR

Following transcardial perfusion with 10 ml of PBS (n = 8/group/day), the brain was removed and placed in a brain block on ice. Brain tissues were dissected from coronal sections spanning 1 mm rostral and 2 mm caudal to the injection sites. A transverse cut was made connecting the most ventral tips of the corpus callosum to remove the ventral portion of the brain and a sagittal cut made to separate the hemispheres. These samples comprised the corpus callosum, overlaying cortex and a minor portion (~10%) of the dorsal striatum. Quantitative RT-PCR was performed as described previously (Chedrawe et al., 2018). The following cycling parameters were used: 95 °C × 3 min + (95 °C × 10 s + 60 °C × 10 s + plate reading) × 40 cycles. Analysis of relative mRNA levels was performed using the ΔΔCq method with Bio-Rad Maestro software, using GAPDH and β-actin as reference genes. The following forward (F) and reverse (R) primers were used: TNF-α, F: CAGGCGGTGCCTATGTCTC, R: CGATCACCCCGAAGTTCAGTAG; IFN-γ, F: ATGAACGCTACACACTGCATC, R: CCATCCTTTTGCCAGTTCCTC; IL-

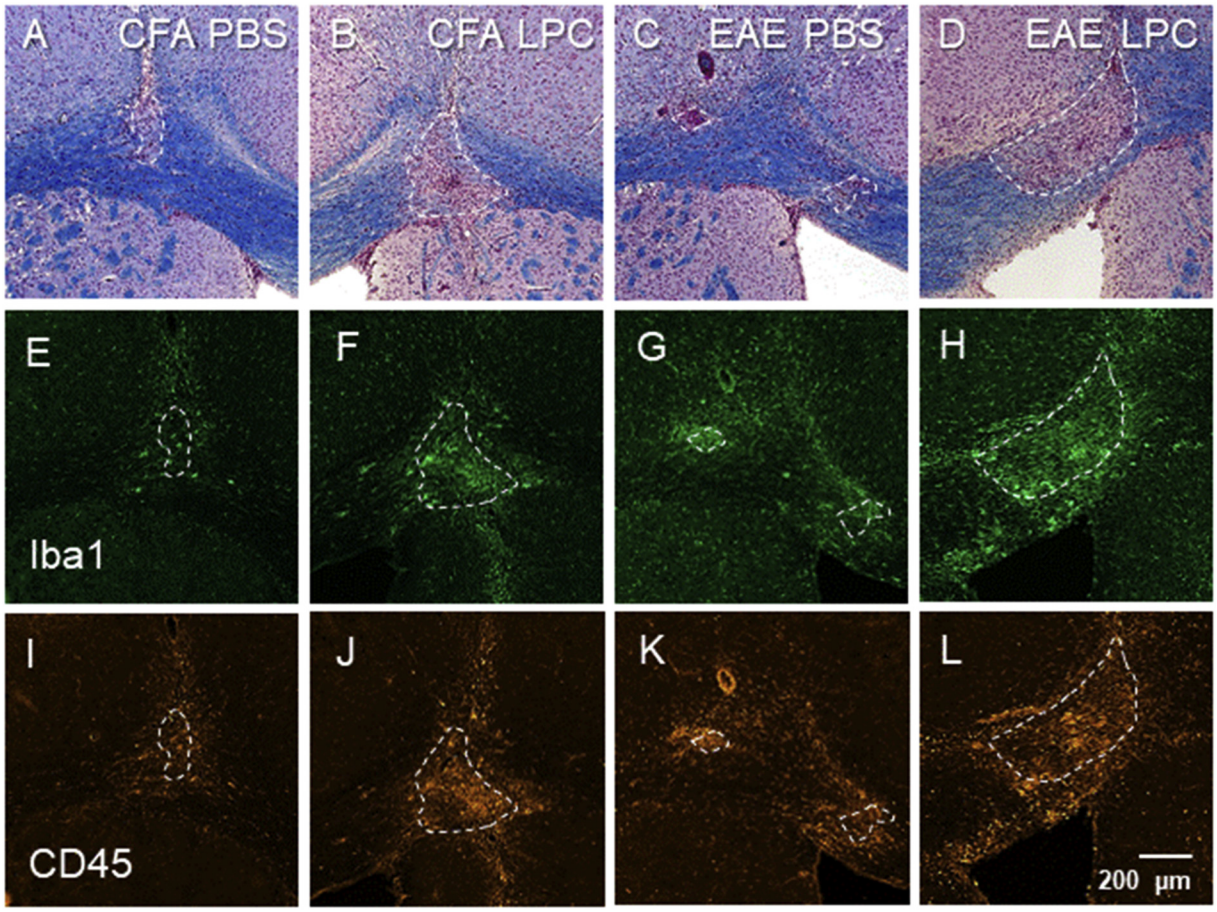

Fig. 3. (A–D) Eriochrome cyanine staining 14 days after the injection of PBS (A and C) and LPC (B and D) injections in the corpus callosum of CFA and EAE mice. Iba1 (E–H) and CD45 (I–L) immunoreactivities in adjacent sections (n = 8 mice/group).

6, F: CTGCAAGAGACTTCCATCCAG, R: AGTGGTATAGACAGGTCTGT TGG; IL-1β, F: GAAATGCCACCTTTTGACAGTG, R: CTGGATGCTCTCA TCAGGACA; TGF-β, F: AGCTGGTGAAACGGAAGCG, R: GCGAGCCTTA GTTTGGACAGG; IL-4, F: GGTCTCAACCCCCAGCTAGT, R: GCCGATGA TCTCTCTCAAGTGAT; GFAP, F: CGGAGACGCATCACCTCTG, R: AGGG AGTGGAGGAGTCATTCG; CD206, F: TCAGCTATTGGACGCGAGGCA, R: AGGGAGTGGAGGAGTCATTCG; GAPDH, F: AGGTCGGTGTGAACG GATTTG, R: GGGGTCGTTGATGGCAACA; β-actin, F: GTGACGTTGAC ATCCGTAAAGA, R: GCCGGACTCATCGTACTCC.

3. Results and discussion

The experimental group of mice were subjected to $MOG_{35–55}$-induced experimental autoimmune encephalomyelitis (EAE) and received bilateral injections of phosphate buffered saline (PBS) and lysophosphatidylcholine (LPC) in the corpus callosum 7 days later (EAE-LPC mice). EAE-LPC mice displayed a typical disease onset between days 9–13 and severity comparable to our historical data for EAE animals which did not receive injections of PBS and LPC (data not shown). $MOG_{35–55}$-immunization controls received injections of CFA and pertussis toxin but not $MOG_{35–55}$ (CFA mice) followed by bilateral injection of PBS and LPC in the corpus callosum 7 days later (CFA-LPC mice). These CFA-LPC animals did not develop any signs of motor impairment (data not shown). Volumetric measurements of EC/NR stained sections for CFA controls mice (Fig. 1A, E and I) and EAE mice (Fig. 1C, G and K) indicated that EAE doubled the size of PBS lesions at day 2, 7 and 14 (Fig. 1N). Relative to CFA controls, EC/NR staining showed that remyelination is accelerated in the LPC lesions of EAE mice (Fig. 1). Immunohistochemical labelling of macrophages/microglial (Iba1) and leukocytes (CD45) revealed that immune infiltration and activation were both elevated in the parenchyma surrounding lesions in EAE mice compared to CFA mice 7 days following PBS/LPC injection (Fig. 2). Immunostaining for the same markers 14 days following PBS/LPC injection showed immune infiltration and activation was still enhanced in the parenchyma of EAE mice but reduced compared to day 7 (Fig. 3). These results are consistent with the possibility that EAE enhanced the rate of myelin repair by increasing the clearance of myelin debris by macrophages and microglia essential for efficient remyelination (Lampron et al., 2015). However, this vigorous innate immune response also appeared to exacerbate damage in the corpus callosum as suggested by incomplete remyelination in EAE mice relative to CFA controls at day 14 (Fig. 1).

Our qRT-PCR data provide insights into the potential mechanisms that accelerate remyelination but also compromise full myelin repair in EAE mice. TNF-α, IFN-γ, IL-1β and IL-6 mRNA levels were elevated in the PBS lesions of EAE mice relative to CFA controls (Fig. 4). The results suggest that mechanical damage produced by the injection of PBS into the corpus callosum produced a greater immune response in EAE mice and support previous findings showing that EAE promotes immune activation in the forebrain (Chanaday and Roth, 2016). TNF-α and IFN-γ mRNA levels were elevated 5-fold while IL-1β mRNA levels doubled in the LPC lesions of EAE relative to CFA mice (Fig. 4). TNF-α exerts dual effects on cell death and survival by activating two TNF receptors (TNFR). TNFR1 mobilizes the innate immune system and promotes the death of multiple neural cell subtypes (Probert, 2015). TNFR2 activation opposes TNFR1 stimulation by inducing a prolonged increase in NF-κB transcriptional activity that is neural protective (Beyer and MacBeath, 2012; Pegoretti et al., 2018). TNFR2 activation also

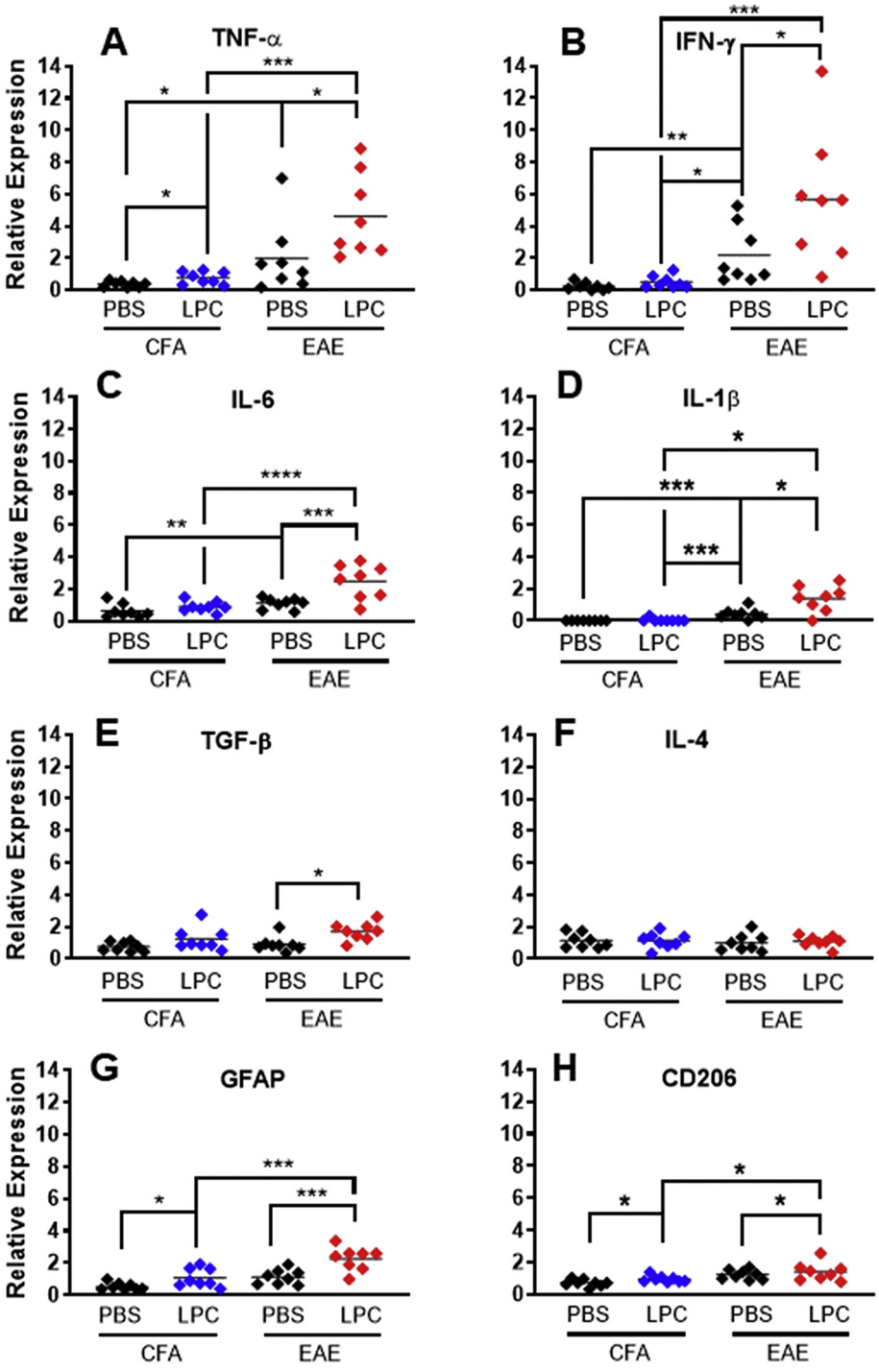

Fig. 4. Relative cytokine (TNF-α, IFN-γ, IL-6, IL-1β, TGF-β, IL-4), GFAP and CD206 mRNA levels measured by qRT-PCR in forebrain samples encompassing the PBS or LPC injection sites in the corpus callosum of CFA and EAE mice at day 7. *$p < 0.05$, ***$p < 0.001$, ****$p < 0.0001$, one-way ANOVA followed by Tukey's post hoc test (n = 8 mice/group).

enhances myelin repair by increasing oligodendrogenesis (Arnett et al., 2001; Madsen et al., 2016). The induction of inflammation and oligodendrocyte cell death by IFN-γ is regarded as a major contributing factor to poor remyelination in MS lesions (Lin et al., 2006; Popko and Baerwald, 1999). However, IFN-γ also facilitates remyelination by increasing the removal of myelin debris that suppresses injurious lipid peroxidation (Sosa et al., 2015). Excessive IL-1β production in EAE kills neurons and oligodendrocytes but also promotes remyelination by inducing insulin-like growth factor 1 production (McKenzie et al., 2018). By contrast, IL-4 expression was unchanged and TGF-β was only 2-fold higher in the LPC lesions of EAE than CFA mice (Fig. 4). The induction of TNF-α, IFN-γ, IL-1β and IL-6 in the LPC lesions of EAE mice that drives demyelination was therefore not matched by a concordant elevation of IL-4 and TGF-β necessary for the resolution of inflammation and myelin repair (Miron et al., 2013).

These findings have clear implications for the elucidation of immune processes that regulate myelin repair. We propose that subjecting genetic mouse lines with various alterations in cytokine signaling to this dual EAE/LPC model would be useful in this regard. Therapeutic screening in this dual EAE/LPC model also provides a new method to

prioritize putative remyelinating and neuroprotective agents for clinical testing in MS. Future studies should employ electron microscopy to assess the effects on EAE on axonal injury and further characterize remyelination after bilateral PBS and LPC injections in the corpus callosum.

Acknowledgements

This work was supported by funding from the MS Society of Canada (EGID 2983).

References

Arnett, H.A., Mason, J., Marino, M., Suzuki, K., Matsushima, G.K., Ting, J.P., 2001. TNF alpha promotes proliferation of oligodendrocyte progenitors and remyelination. Nat. Neurosci. 4, 1116–1122.

Beyer, E.M., MacBeath, G., 2012. Cross-talk between receptor tyrosine kinase and tumor necrosis factor-alpha signaling networks regulates apoptosis but not proliferation. Mol. Cell. Proteomics 11, M111.

Chanaday, N.L., Roth, G.A., 2016. Microglia and astrocyte activation in the frontal cortex of rats with experimental autoimmune encephalomyelitis. Neuroscience 314, 160–169.

Chedrawe, M.A.J., Holman, S.P., Lamport, A.C., Akay, T., Robertson, G.S., 2018. Pioglitazone is superior to quetiapine, clozapine and tamoxifen at alleviating experimental autoimmune encephalomyelitis in mice. J. Neuroimmunol. 321, 72–82.

Duncan, I.D., Brower, A., Kondo, Y., Curlee Jr., J.F., Schultz, R.D., 2009. Extensive remyelination of the CNS leads to functional recovery. Proc. Natl. Acad. Sci. U. S. A. 106, 6832–6836.

Fancy, S.P., Kotter, M.R., Harrington, E.P., Huang, J.K., Zhao, C., Rowitch, D.H., Franklin, R.J., 2010. Overcoming remyelination failure in multiple sclerosis and other myelin disorders. Exp. Neurol. 225, 18–23.

Franklin, R.J., 2002. Why does remyelination fail in multiple sclerosis? Nat. Rev. Neurosci. 3, 705–714.

Franklin, R.J., Gallo, V., 2014. The translational biology of remyelination: past, present, and future. Glia 62, 1905–1915.

Frischer, J.M., Bramow, S., Dal-Bianco, A., Lucchinetti, C.F., Rauschka, H., Schmidbauer, M., Laursen, H., Sorensen, P.S., Lassmann, H., 2009. The relation between inflammation and neurodegeneration in multiple sclerosis brains. Brain 132, 1175–1189.

Hall, S.M., 1972. The effect of injections of lysophosphatidyl choline into white matter of the adult mouse spinal cord. J. Cell Sci. 10, 535–546.

Henderson, A.P., Barnett, M.H., Parratt, J.D., Prineas, J.W., 2009. Multiple sclerosis: distribution of inflammatory cells in newly forming lesions. Ann. Neurol. 66, 739–753.

Hoflich, K.M., Beyer, C., Clarner, T., Schmitz, C., Nyamoya, S., Kipp, M., Hochstrasser, T., 2016. Acute axonal damage in three different murine models of multiple sclerosis: a comparative approach. Brain Res. 1650, 125–133.

Jones, M.V., Nguyen, T.T., Deboy, C.A., Griffin, J.W., Whartenby, K.A., Kerr, D.A., Calabresi, P.A., 2008. Behavioral and pathological outcomes in MOG 35-55 experimental autoimmune encephalomyelitis. J. Neuroimmunol. 199, 83–93.

Keough, M.B., Jensen, S.K., Yong, V.W., 2015. Experimental demyelination and remyelination of murine spinal cord by focal injection of lysolecithin. J. Vis. Exp. 97, 1–8.

Lampron, A., Larochelle, A., Laflamme, N., Prefontaine, P., Plante, M.M., Sanchez, M.G., Yong, V.W., Stys, P.K., Tremblay, M.E., Rivest, S., 2015. Inefficient clearance of myelin debris by microglia impairs remyelinating processes. J. Exp. Med. 212, 481–495.

Lin, W., Kemper, A., Dupree, J.L., Harding, H.P., Ron, D., Popko, B., 2006. Interferon-gamma inhibits central nervous system remyelination through a process modulated by endoplasmic reticulum stress. Brain 129, 1306–1318.

Madsen, P.M., Motti, D., Karmally, S., Szymkowski, D.E., Lambertsen, K.L., Bethea, J.R., Brambilla, R., 2016. Oligodendroglial TNFR2 mediates membrane TNF-dependent repair in experimental autoimmune encephalomyelitis by promoting oligodendrocyte differentiation and remyelination. J. Neurosci. 36, 5128–5143.

McKenzie, B.A., Mamik, M.K., Saito, L.B., Boghozian, R., Monaco, M.C., Major, E.O., Lu, J.Q., Branton, W.G., Power, C., 2018. Caspase-1 inhibition prevents glial inflammasome activation and pyroptosis in models of multiple sclerosis. Proc. Natl. Acad. Sci. U. S. A. 115, E6065–E6074.

Miron, V.E., Boyd, A., Zhao, J.W., Yuen, T.J., Ruckh, J.M., Shadrach, J.L., van, W.P., Wagers, A.J., Williams, A., Franklin, R.J., Ffrench-Constant, C., 2013. M2 microglia and macrophages drive oligodendrocyte differentiation during CNS remyelination. Nat. Neurosci. 16, 1211–1218.

Pegoretti, V., Baron, W., Laman, J.D., Eisel, U.L.M., 2018. Selective modulation of TNF-TNFRs signaling: insights for multiple sclerosis treatment. Front. Immunol. 9, 925.

Popko, B., Baerwald, K.D., 1999. Oligodendroglial response to the immune cytokine interferon gamma. Neurochem. Res. 24, 331–338.

Probert, L., 2015. TNF and its receptors in the CNS: the essential, the desirable and the deleterious effects. Neuroscience 302, 2–22.

Schultz, V., van der Meer, F., Wrzos, C., Scheidt, U., Bahn, E., Stadelmann, C., Bruck, W., Junker, A., 2017. Acutely damaged axons are remyelinated in multiple sclerosis and experimental models of demyelination. Glia 65, 1350–1360.

Sosa, R.A., Murphey, C., Robinson, R.R., Forsthuber, T.G., 2015. IFN-gamma ameliorates autoimmune encephalomyelitis by limiting myelin lipid peroxidation. Proc. Natl. Acad. Sci. U. S. A. 112, E5038–E5047.

Steinman, L., Zamvil, S.S., 2006. How to successfully apply animal studies in experimental allergic encephalomyelitis to research on multiple sclerosis. Ann. Neurol. 60, 12–21.

Trapp, B.D., Stys, P.K., 2009. Virtual hypoxia and chronic necrosis of demyelinated axons in multiple sclerosis. Lancet Neurol. 8, 280–291.

Trapp, B.D., Peterson, J., Ransohoff, R.M., Rudick, R., Mork, S., Bo, L., 1998. Axonal transection in the lesions of multiple sclerosis. N. Engl. J. Med. 338, 278–285.

Warford, J.R., Lamport, A.C., Clements, D.R., Malone, A., Kennedy, B.E., Kim, Y., Gujar, S.A., Hoskin, D.W., Easton, A.S., 2018. Surfen, a proteoglycan binding agent, reduces inflammation but inhibits remyelination in murine models of multiple sclerosis. Acta Neuropathol. Commun. 6, 4.